Catalysis Science & Technology

ROYAL SOCIETY OF CHEMISTRY

PAPER

View Article Online
View Journal | View Issue





Cite this: *Catal. Sci. Technol.*, 2020, **10**, 1739

# Enhanced propane dehydrogenation to propylene over zinc-promoted chromium catalysts

Jie Liu,†[abc] Yong Liu,†[ab] Youming Ni,[ab] Hongchao Liu,[ab] Wenliang Zhu*[ab] and Zhongmin Liu*[ab]

Received 23rd September 2019,
Accepted 15th January 2020

DOI: 10.1039/c9cy01921a

rsc.li/catalysis

Direct propane dehydrogenation (PDH) is an attractive technology for propylene production. We show here that propane conversion is significantly enhanced by the addition of ZnO to $Cr_2O_3$. Furthermore, its activity is strongly dependent on the Zn/Cr molar ratio and one with Zn/Cr = 0.3 gives the highest propane conversion and propylene selectivity among the studied $Zn_xCr$ catalysts ($x$ denoting the molar ratio, 0–0.5). Characterization with X-ray diffraction, nitrogen physisorption, X-ray fluorescence spectroscopy, temperature-programmed reduction, temperature-programmed desorption, transmission electron microscopy, and X-ray photoelectron spectroscopy indicates that addition of zinc to $Cr_2O_3$ leads to formation of a spinel phase and reduction of the particle size, and hence forms more defect sites. The Arrhenius plots suggest that the apparent activation energy of the PDH reaction is significantly lowered over $Zn_{0.3}Cr$.

## Introduction

Propylene is an important and basic building block in the chemical industry, and is employed for the production of polymers, oxygenates and other chemical compounds.[1–3] Currently, propylene is commercially manufactured by steam cracking, fluid catalytic cracking (FCC) and the methanol-to-olefin (MTO) process.[4–6] With the rapidly growing demand for propylene and the availability of large reserves of shale gas, direct propane dehydrogenation (PDH) to propylene has become an attractive alternative process for production of propylene.[7,8]

Cr-Based catalysts have been extensively studied for the PDH reaction since the first report by Frey and Huppke.[9] A wide range of Cr-based catalysts have been examined including $Cr/Al_2O_3$, $Cr/SiO_2$, and $Cr/ZrO_2$.[10–12] De Rossi *et al.* reported highly selective $Cr/Al_2O_3$ and $Cr/SiO_2$ catalysts for PDH in the temperature range of 723–823 K. However, these catalysts underwent a deactivation process with time on stream and their activity was still low.[11] For the most frequently studied $Cr/Al_2O_3$ catalyst, its selectivity needs to be improved due to the side reactions such as cracking and coking over the surface acid sites of $Al_2O_3$, hence leading to reduced propane conversion and propylene selectivity. Therefore, great efforts have been made to improve the performance of the $Cr/Al_2O_3$ catalyst by use of different promoters, preparation methods and support materials.[13,14] Fujdala *et al.* synthesized Cr/Si/Al/O and Cr/Si/Zr/O catalysts *via* a cothermolysis method capable of exhibiting propane conversion above 35% and propylene selectivity greater than 95% at 723 K in the PDH reaction.[13] In the typical CATOFIN process, $\gamma$-$Al_2O_3$-supported catalysts contained 18–20 wt% $CrO_x$ promoted by 1–2 wt% Na or K.[15] In addition, other catalysts based on V, Ga, Zr and Zn have also been investigated for the PDH reaction.[16–19] Among them, Zn-based catalysts were thought to be promising due to their low cost and high catalytic performance in PDH.[20] Chen *et al.* reported that small ZnO nanoclusters supported on a dealuminated β zeolite showed high catalytic activity and propylene selectivity in the PDH reaction.[20] Schweitzer *et al.* found that coordinatively unsaturated $Zn^{2+}$ supported on silica exhibited Lewis acid properties and could catalyze the PDH reaction with a high propylene selectivity of more than 95%.[21] Therefore, the issue whether zinc oxide is an effective promoter for Cr-based catalysts in the PDH reaction is worthy to be explored.

Zn–Cr based oxides are typical methanol synthesis catalysts from syngas derived from coal, natural gas and biomass at relatively high reaction temperature and are also employed for other reactions. Tian *et al.* reported a Zn–Cr catalyst with a Zn/Cr element ratio of 1 : 1 exhibited an outstanding isobutanol synthesis activity from syngas.[22] Al-Wadaani *et al.* studied Zn–Cr catalysts with a wide range of Zn/Cr ratios (20/1–1/30) for dehydroisomerisation of α-pinene to *p*-cymene and one with a Zn/Cr ratio of 1 : 1 showed the highest yield.[23] According to X-ray diffraction (XRD)

[a] *National Engineering Laboratory for Methanol to Olefins, Dalian Institute of Chemical Physics, Chinese Academy of Sciences, Dalian 116023, China. E-mail: wlzhu@dicp.ac.cn, liuzm@dicp.ac.cn*
[b] *Dalian National Laboratory for Clean Energy, Dalian Institute of Chemical Physics, Chinese Academy of Sciences, Dalian 116023, China*
[c] *University of Chinese Academy of Sciences, Beijing 100049, China*
† These authors contributed equally to this work.

measurements of Zn–Cr mixed oxides used in these reactions, the catalysts have a Zn–Cr spinel phase with an excess of $Zn^{2+}$ cations. Bertoldi *et al.* proposed that the excess $Zn^{2+}$ located at the octahedral sites, which were coordinatively unsaturated, had a remarkable adsorptive capacity towards CO and other molecules, resulting in high catalytic performance.[24] However, little research has been done on Zn–Cr mixed oxides with excess $Cr^{3+}$ and Zn–Cr based oxides were not yet studied for the PDH reaction.

Therefore, we prepared a series of Zn–Cr mixed oxides with different Zn/Cr molar ratios (0–0.5) as catalysts for the PDH reaction. Interestingly, these bi-component oxides are active in the PDH reaction and the catalyst $Zn_{0.3}Cr$ shows the highest activity with 31.3% propane conversion and around 94% propylene selectivity. Detailed characterization studies were carried out and revealed that the excellent performance of Zn–Cr mixed oxides in the PDH reaction could be attributed to the formation of a small-size Zn–Cr spinel with defect sites.

# Experimental

### Catalyst preparation

$Zn_xCr$ oxides ($x$ = 0.1, 0.3, 0.5) were prepared by a co-precipitation method, with $x$ standing for the molar ratio of Zn/Cr. Taking the $Zn_{0.3}Cr$ sample as an example, the following synthesis procedure was used. 0.03 mol $Zn(NO_3)_2{\cdot}6H_2O$ and 0.10 mol $Cr(NO_3)_3{\cdot}9H_2O$ were dissolved in a certain amount of deionized water to form a solution having a concentration of 1 mol $L^{-1}$. A 200 ml aqueous solution with 0.2 mol $(NH_4)_2CO_3$ was used as a precipitant. The aforementioned solutions were simultaneously added into a beaker containing 200 ml deionized water under stirring at 70 °C. During the process, the pH of the suspension was controlled between 7.0 and 7.1. The suspension was then aged for 3 h at 70 °C under stirring, followed by filtration and washing with deionized water three times. The resulting sample was dried at 100 °C for 12 h and then calcined at 500 °C in air for 4 h. ZnO, $Cr_2O_3$ and other $Zn_xCr$ samples were prepared by following the same procedure under the same conditions.

For comparison, $CrO_x/Al_2O_3$ was prepared by incipient wetness impregnation of $Al_2O_3$ with a $Cr(NO_3)_3{\cdot}9H_2O$ aqueous solution.[25] After impregnation, the sample was dried at 120 °C overnight and then calcined at 550 °C in air for 4 h. The actual concentration of $Cr_2O_3$ in the prepared catalyst is 17 wt%.

### Catalyst characterization

The BET surface areas were obtained by nitrogen physisorption on a Micromeritics ASAP 2020 system at 77 K. Prior to measurements, the samples were degassed at 625 K for 4 h. The chemical composition of all the samples was determined by XRF on a Philips Magix-601 XRF spectrometer.

The crystal phases of the samples were characterized by XRD, which was performed on a PANalytical X'Pert PRO X-ray diffractometer with Cu Kα radiation. The crystallite sizes were calculated by the Scherrer equation. The particle size was also estimated by TEM, which was performed on a JEM-2100 microscope operating at 200 kV. Energy dispersive spectroscopy (EDS) spectra were obtained on a JEM-2100F microscope operating at 200 kV.

XPS was performed on an ESCALAB 250Xi spectrometer with monochromatized Al Kα as the exciting radiation. The binding energy of contaminant carbon C1s at 284.8 eV was used as a reference. *In situ* XPS was performed on a SPECS EnviroESCA spectrometer. 10 mbar 5% $C_3H_8$/Ar was introduced into the sample at 480 °C, before and after which the XPS spectra of the sample were measured.

The reducibility was characterized by $H_2$-TPR, which was performed on a Micromeritics AutoChem 2920 analyzer. The samples were firstly treated in flowing Ar at 150 °C for 1 h before the test. After that, the samples were reduced in 10% $H_2$/Ar flow at a heating rate of 10 °C $min^{-1}$. $NH_3$-TPD was also carried out on the Micromeritics AutoChem 2920 analyzer. Before the measurement, the sample was firstly treated in flowing He at 450 °C for 1 h. Then, 10% $NH_3$/He was introduced into the sample at 100 °C for 30 min followed by flushing with He. Subsequently, the sample was heated in He at a rate of 10 °C $min^{-1}$ while $NH_3$ desorption was monitored using a TCD detector.

### Catalytic activity measurement

PDH reactions were performed in a fixed-bed stainless steel reactor fitted with a quartz lining. 0.3 g of the catalyst was loaded and heated to 400 °C for 1 h and 480 °C for 30 min in $N_2$ (30 ml $min^{-1}$). A mixture of 5% $C_3H_8$ and 95% Ar was fed into the reactor at a flow rate of 25 ml $min^{-1}$. The reaction was monitored after 5 min from the start and was allowed to proceed for 5 h. Effluents were analysed with an on-line Agilent 7890B gas chromatograph, which was equipped with a thermal conductivity detector (TCD) and a flame ionization detector (FID). Propane conversion ($X_{C_3H_8}$) and propylene selectivity ($S_{C_3H_6}$) were calculated on a carbon atom basis and were expressed as the following:

$$X_{C_3H_8} = \frac{\sum F_i \times A_i}{\sum F_i \times A_i + F_{C_3H_8} \times A_{C_3H_8}}$$

$$S_{C_3H_6} = \frac{F_i \times A_i}{\sum F_i \times A_i}$$

$$F_i = f_i \times n_i,$$

Among these, $f_i$ stands for the molar correction factor of the product i, $n_i$ is the carbon number of the product i, and $A_i$ refers to the peak area of the product i measured by FID.

# Results and discussion

The performance of all the catalysts for the PDH reaction was evaluated at 480 °C, 0.1 MPa, 5% $C_3H_8$/Ar and a space velocity of 5000 ml $h^{-1}$ $g_{cat}^{-1}$. Upon addition of Zn, the activity improves obviously. However, there appears to be an

 

optimum range of Zn addition. Among all the catalysts tested, $Zn_{0.3}Cr$ exhibits the optimal activity. As shown in Fig. 1, an initial conversion of 21% over $Zn_{0.3}Cr$ is obtained and further increases to 31.3% with time on stream, which is much higher than that of 7% over $Zn_{0.1}Cr$ and 11% over $Zn_{0.5}Cr$. Meanwhile, the $Zn_{0.3}Cr$ catalyst also exhibits the highest selectivity to propylene, with $S_{C_3H_6}$ maintaining around 94% along time on stream up to 300 min. Methane and $C_4$ hydrocarbons are the main by-products for $Zn_{0.3}Cr$ with very little ethylene and ethane (Fig. 1c). For comparison, the single components $Cr_2O_3$ and ZnO were used as catalysts for the PDH reaction under the same reaction conditions. Fig. 1a shows that $Cr_2O_3$ gives a propane conversion of about 10% initially and drops rather quickly to around 5% and then levels off with a propylene selectivity of around 88%, which is lower than $Zn_{0.3}Cr$. By contrast, ZnO is much less active, with $X_{C_3H_8}$ lower than 2%, demonstrating the weak ability of ZnO to activate propane. In addition, $Cr_2O_3/Al_2O_3$, which has been frequently studied, was synthesized for comparison. The impregnation method was employed and the $Cr_2O_3$ loading was 17 wt%. Fig. 1d shows that its PDH activity under the same conditions is much lower than the $Zn_{0.3}Cr$ catalyst as its propane conversion is only 9% after reaching steady state.

To understand the origin of the high activity of $Zn_{0.3}Cr$, we prepared a physically mixed ZnO–$Cr_2O_3$ catalyst with single components ZnO and $Cr_2O_3$ with the same molar ratio of Zn/Cr = 0.3 (denoted as ZnO–$Cr_2O_3$). One sees that $X_{C_3H_8}$ is only 3%, which is similar to that obtained over ZnO, lower than that obtained over $Cr_2O_3$, and one order of magnitude lower than that on $Zn_{0.3}Cr$ (Fig. 1d). These results suggest that the high activity of the $Zn_{0.3}Cr$ catalyst could not be solely attributed to the coexisting ZnO and $Cr_2O_3$. Therefore, we turned to understanding the physicochemical properties of the $Zn_xCr$ catalysts in comparison to references ZnO and $Cr_2O_3$.

XRD was carried out in order to identify the crystal phase structure of the catalysts and the results are shown in Fig. 2a.

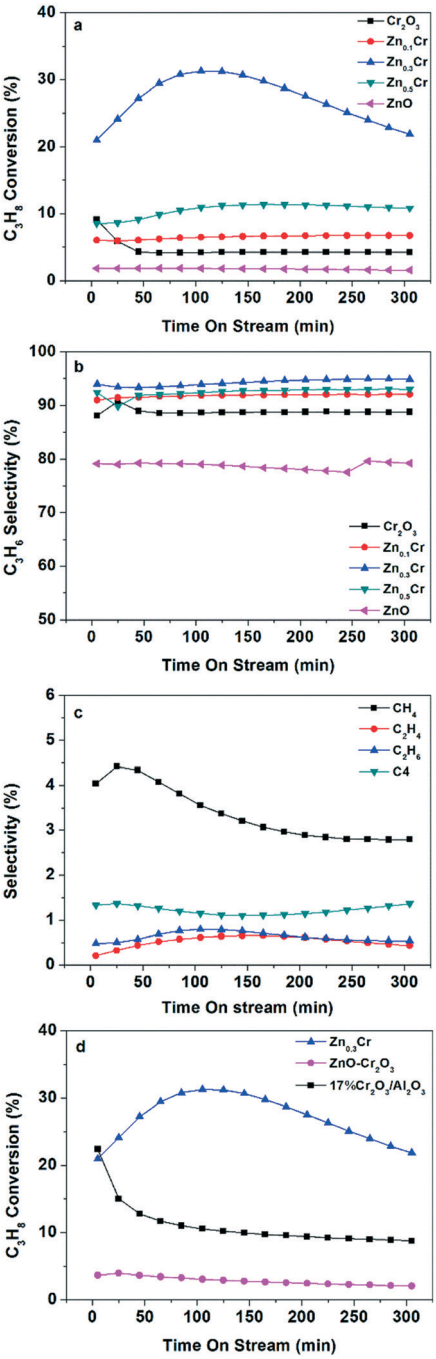


**Fig. 1** Catalytic performance of different catalysts in the propane dehydrogenation reaction. (a) Propane conversion; (b) selectivity to propylene; (c) selectivity to by-products for $Zn_{0.3}Cr$; (d) the activity of $Zn_{0.3}Cr$ in comparison with a physical mixture of ZnO–$Cr_2O_3$ and 17% $Cr_2O_3/Al_2O_3$. Reaction conditions: $T$ = 480 °C, $P$ = 0.1 MPa, GHSV = 5000 ml $h^{-1}$ $g_{cat}^{-1}$, $C_3H_8$/Ar = 5/95.

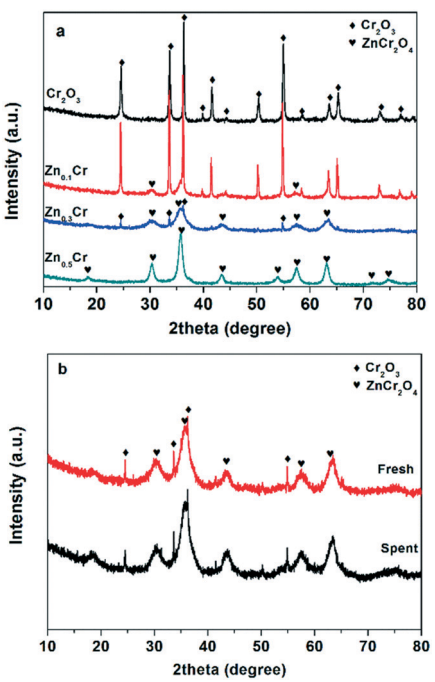


**Fig. 2** XRD patterns of the (a) Cr-containing catalysts and (b) $Zn_{0.3}Cr$ sample before and after the reaction.

The single component catalyst $Cr_2O_3$ exhibits only the crystal phase of $Cr_2O_3$ with an average crystal size of 32.8 nm, estimated according to the Scherrer equation, as listed in Table 1. With the addition of Zn to $Cr_2O_3$ at Zn/Cr = 0.1, the diffraction peaks of $ZnCr_2O_4$ appear in addition to those of $Cr_2O_3$ and the crystal size of $ZnCr_2O_4$ is estimated to be 7.9 nm. At Zn/Cr = 0.3, the intensity of $Cr_2O_3$ reduces further and the diffraction peaks of the $ZnCr_2O_4$ phase become more prominent but still rather broad. Interestingly, the estimated crystal size of the $ZnCr_2O_4$ phase becomes smaller (4.8 nm) with respect to that over $Zn_{0.1}Cr$, but the remaining $Cr_2O_3$ crystals still retain a large size. At Zn/Cr = 0.5, there is only the $ZnCr_2O_4$ spinel phase detected and its crystal size increases to 8.8 nm compared to $Zn_{0.3}Cr$. It is noted that the crystal structure does not change after the reaction, as evidenced by the XRD pattern of the spent $Zn_{0.3}Cr$ catalyst (Fig. 2b).

Smaller particles generally result in a higher surface area, as evidenced by the textual properties of these catalysts (Table 1). The specific surface areas and pore volumes of the bi-component catalysts $Zn_xCr$ are much higher. They are 43.0 $m^2\ g^{-1}$ and 0.11 $cm^3\ g^{-1}$ for $Zn_{0.1}Cr$, and 148.4 $m^2\ g^{-1}$ and 0.29 $cm^3\ g^{-1}$ for $Zn_{0.3}Cr$. However, further increasing the Zn/Cr ratio to 0.5 leads to a reduced specific surface area and pore volume (85.0 $m^2\ g^{-1}$ and 0.19 $cm^3\ g^{-1}$), consistent with the crystal size.

Further characterization with HRTEM (Fig. 3) shows that the particle size of the $Cr_2O_3$ catalyst is not uniform, with an average size of around 75.7 nm. The $Zn_{0.1}Cr$ and $Zn_{0.3}Cr$ catalysts show two different phases, *i.e.* $Cr_2O_3$ and $ZnCr_2O_4$, consistent with the XRD results. Interestingly, the particle size of the $ZnCr_2O_4$ phase is rather uniform being around 7.3 nm, whereas the $Cr_2O_3$ phase is composed of large particles around 100 nm for $Zn_{0.1}Cr$. The particle size of $ZnCr_2O_4$ decreases to 6.2 nm for $Zn_{0.3}Cr$. There are only few $Cr_2O_3$ particles observed. In comparison, HRTEM validates that $Zn_{0.5}Cr$ merely exhibits the $ZnCr_2O_4$ crystal phase and the particles are rather uniform but the size increases further to around 11.6 nm with respect to $Zn_{0.3}Cr$. The above results indicate that the addition of zinc to $Cr_2O_3$ leads to the formation of a $ZnCr_2O_4$ spinel phase with particle size lower than 10 nm, whereas the $Cr_2O_3$ phase in the bi-component catalysts $Zn_xCr$ still retains a bulky particle size larger than 50 nm. Among them, the $ZnCr_2O_4$ phase in $Zn_{0.3}Cr$ has the smallest size being 4.8 nm. Generally, smaller particles give a higher surface area, and thus it is understandable that $Zn_{0.3}Cr$ exhibits the highest surface area. Furthermore, the EDS mappings of the $ZnCr_2O_4$ phase in the $Zn_{0.3}Cr$ catalyst in Fig. 4 show that the Zn and Cr elements are evenly distributed. Besides, the Zn/Cr molar ratio is 0.32 measured by EDS analysis, in agreement with the value measured by XRF (0.29). Therefore, the remarkably enhanced PDH activity is likely related to the formation of small sized Zn–Cr spinel species because smaller particles are frequently accompanied by defects.

Defect sites on oxides usually exhibit Lewis acidic properties and $NH_3$-TPD is frequently employed to characterize the properties.[18,26] It is generally accepted that the position and area of the ammonia desorption peak are directly associated with the acid strength and the acid amount, respectively.[26] As shown in Fig. 5a, there are several $NH_3$ desorption peaks for $Zn_xCr$ mixed oxides, implying the presence of multiple types of defect sites with different binding strengths to $NH_3$. These peaks fall in a similar temperature range for the three $Zn_xCr$ samples. It appears that the $Zn_{0.3}Cr$ sample has another strong peak emerging beyond 400 °C. A blank temperature programmed experiment in He under the same conditions suggests that the decomposition of the catalyst itself has some contribution to the signal after 500 °C since it was calcined at 500 °C, as shown in Fig. 5b. $NH_3$-TPD further shows that the amount of $NH_3$ desorbed from $Zn_{0.3}Cr$ is considerably higher than that from the other two, as listed in Table 2. Tian *et al.* studied Zn–Cr spinel catalysts with excessive Zn ($Zn_{0.8}Cr$ and $Zn_{1.2}Cr$) for isobutanol synthesis from syngas and they pointed out that the acidic character over these Zn–Cr spinel catalysts characterized by $NH_3$-TPD was closely related to their surface properties. The higher peak area reflects the presence of more defect sites.[27,28] Although non-stoichiometric spinels with excessive Zn have been widely studied for methanol and higher alcohol synthesis,[24,27,28] Zn-deficient spinels were rarely studied. Elucidation of the actual structures of these defects will require more sophisticated experimental and theoretical studies.

Gao *et al.* reported that the metastable structure of non-stoichiometric Zn–Cr spinels with cation disorder and many defects could be stabilized by hydroxyl groups.[29] Therefore, we studied the surface hydroxyl by XPS. As shown in Fig. 6, the signal at a low binding energy of 530.3–530.7 eV is assigned to lattice oxygen (labeled as $O_{latt}$) and the signal at a higher binding energy of 531.9–532.2 eV is derived from surface hydroxyl groups (labeled as $O_{OH}$), as reported previously.[29,30] The ratio of $(O_{OH})/(O_{latt} + O_{OH})$ is estimated and summarized

**Table 1** Textural properties of different catalysts

| Catalysts | Zn/Cr atomic ratio[a] | BET surface area ($m^2\ g^{-1}$) | Pore volume ($cm^3\ g^{-1}$) | Average diameter[b] (nm) | | Average diameter[c] (nm) | |
|---|---|---|---|---|---|---|---|
| | | | | $Cr_2O_3$ | $ZnCr_2O_4$ | $Cr_2O_3$ | $ZnCr_2O_4$ |
| $Cr_2O_3$ | — | 9.5 | 0.03 | 32.8 | — | 75.7 | — |
| $Zn_{0.1}Cr$ | 0.11 | 43.0 | 0.11 | 53.6 | 7.9 | 104.0 | 7.3 |
| $Zn_{0.3}Cr$ | 0.29 | 148.4 | 0.29 | 61.7 | 4.8 | — | 6.2 |
| $Zn_{0.5}Cr$ | 0.54 | 85.0 | 0.19 | — | 8.8 | — | 11.6 |
| ZnO | — | 11.8 | 0.03 | — | — | — | — |

[a] Zn/Cr atomic ratio was measured by XRF. [b] Crystallite size was calculated by the Scherrer equation based on XRD. [c] Average particle size was determined by TEM.

 

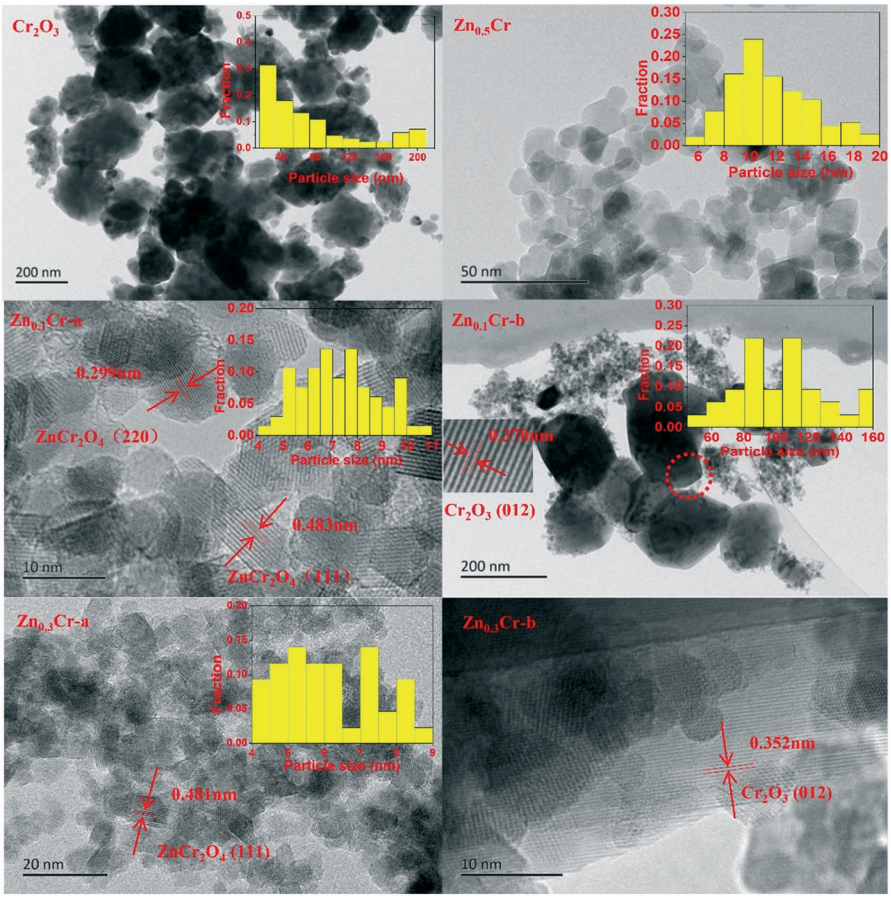


Fig. 3 TEM images of the Cr-containing catalysts with the images labelled a referring to the $ZnCr_2O_4$ phase and images labelled b referring to the $Cr_2O_3$ phase.

in Table 2. For the Zn–Cr oxides, the ratio of $(O_{OH})/(O_{latt} + O_{OH})$ increases from 27.6% to 33.9% when the Zn/Cr molar ratio increases from 0.1 to 0.3, and then decreases to 29.6% when the Zn/Cr molar ratio further increases to 0.5. These data further validate the presence of more defect sites in the small-size Zn–Cr spinel of the $Zn_{0.3}Cr$ catalyst.

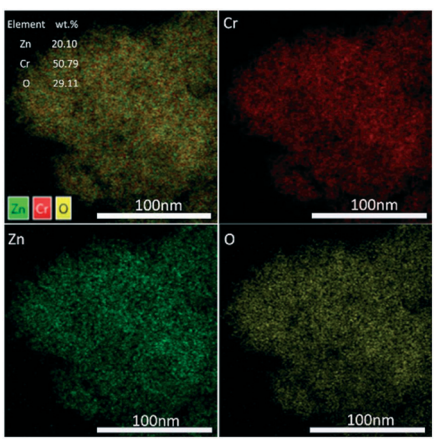


Fig. 4 EDS mappings of the Zn–Cr spinel phase in the $Zn_{0.3}Cr$ catalyst.

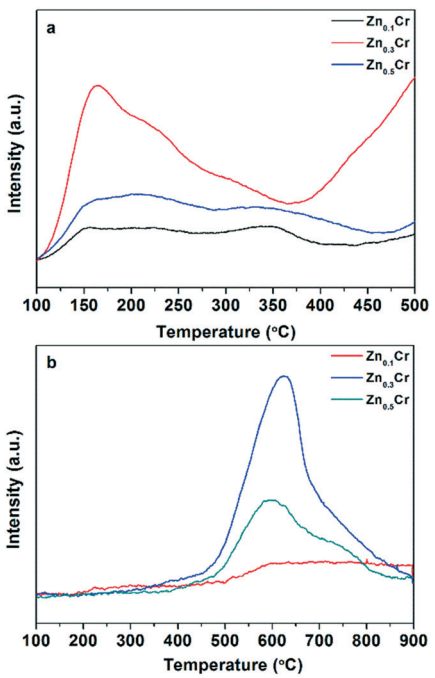


Fig. 5 Temperature-programmed desorption profiles of catalysts with different Zn/Cr molar ratios. (a) $NH_3$-TPD; (b) blank experiment.

Table 2 The results of $NH_3$-TPD and the O species composition of the $Zn_xCr$ catalysts

| Catalysts | Peaks of acid sites (°C) | Amount of acid sites (mmol $g^{-1}$) | Total acidity (mmol $g^{-1}$) | $O_{OH}/(O_{latt} + O_{OH})$ |
|---|---|---|---|---|
| $Zn_{0.1}Cr$ | 222, 342 | 0.07, 0.06 | 0.13 | 27.6% |
| $Zn_{0.3}Cr$ | 163 | 0.36 | 0.36 | 33.9% |
| $Zn_{0.5}Cr$ | 203, 234 | 0.14, 0.11 | 0.25 | 29.6% |

In order to further understand the promotion effect of zinc on Cr-based catalysts for the PDH reaction, the apparent activation energy over $Zn_xCr$ catalysts is estimated according to the formation rate of propylene in a temperature range between 480–540 °C. As shown in Fig. 7, the $Zn_{0.3}Cr$ catalyst exhibits a much lower apparent activation energy than the other two catalysts. It indicates that the addition of zinc to $Cr_2O_3$ promotes the active sites in addition to generating the $ZnCr_2O_4$ spinel phase and reducing the particle size.

$H_2$-TPR was conducted to investigate the reducibility of the catalysts and the profiles of the $Zn_xCr$ catalysts are shown in Fig. 8. For comparison, the $H_2$-TPR profiles of the single component $Cr_2O_3$ and ZnO catalysts are also presented. The results show that no obvious reduction peak is observed for ZnO below 650 °C. There is an obvious reduction peak at around 441 °C for $Cr_2O_3$. It was reported that there existed a small amount of $Cr^{6+}$ species over the freshly calcined $Cr_2O_3$ oxides.[31] The reduction peak around 441 °C over $Cr_2O_3$ was likely attributed to the reduction of $Cr^{6+}$ to $Cr^{3+}$, as reported by Akula *et al.*[32] Interestingly, there are two reduction peaks observed for the $Zn_xCr$ oxides and the reduction temperatures (<361 °C) are much lower than for the single component $Cr_2O_3$. This implies the presence of more than one type of chromium species over $Zn_xCr$ oxides. For $Zn_{0.1}Cr$, there are two reduction peaks observed at around 252 and 361 °C, which could be assigned to the reduction of $Cr^{6+}$, from the Zn–Cr spinel phase or partially oxidized $Cr_2O_3$ phase, to $Cr^{3+}$ as reported by Simard *et al.*[33] The Zn and Cr cations within the stoichiometric Zn–Cr spinel (normally $ZnCr_2O_4$) are very difficult to reduce.[34] Therefore, the broad reduction peak in the temperature range of 100–350 °C for $Zn_{0.3}Cr$ and the reduction peaks at around 256 and 300 °C for $Zn_{0.5}Cr$ could be assigned to the surface $Cr_2O_3$ species and/or Zn–Cr spinel phase with defects.[34] Interestingly, the $Zn_{0.3}Cr$ catalyst exhibits the highest hydrogen consumption among all the $Zn_xCr$ catalysts, which is consistent with its highest concentration of defect site $Cr^{3+}$.[22] Lin *et al.* stated that there was a direct relationship between catalytic activity and the reducibility of a catalyst, *i.e.* the higher the reducibility of supported chromium oxide catalysts, the higher the catalytic activity in the dehydrogenation of $C_2H_6$ to $C_2H_4$.[35] Consequently, it is understandable that the $Zn_{0.3}Cr$ catalyst exhibits the highest PDH activity among the studied catalysts.

The $Zn_{0.3}Cr$ catalyst was further characterized by *in situ* XPS. The spectra were taken before propane was fed in and after the reaction had been allowed for 5 and 30 min, respectively. As shown in Fig. 9a, the peaks at 1021.4 and 1044.6 eV are attributed to $Zn^{2+}$,[36] which did not change during the reaction.

The spectra of Cr 2p are shown in Fig. 9b. Deconvolution of the Cr $2p_{3/2}$ spectrum indicates the presence of both $Cr^{6+}$ and $Cr^{3+}$ species over the catalyst before the reaction, represented by the signals at binding energies of 576.8 and 579.3 eV, respectively.[37] However, after the reaction for 5 min at 480 °C, the surface $Cr^{6+}$ species disappear and there are only $Cr^{3+}$ species left. The Cr 2p spectrum of $Zn_{0.3}Cr$ after the

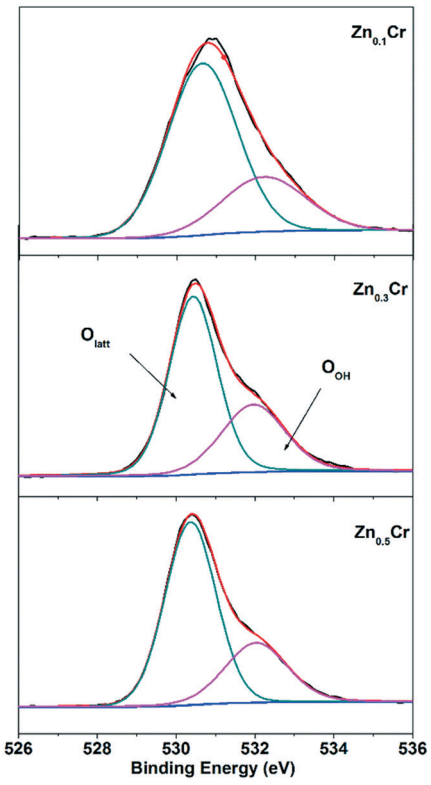


Fig. 6 O 1s XPS spectra of $Zn_xCr$ with different Zn/Cr molar ratios.

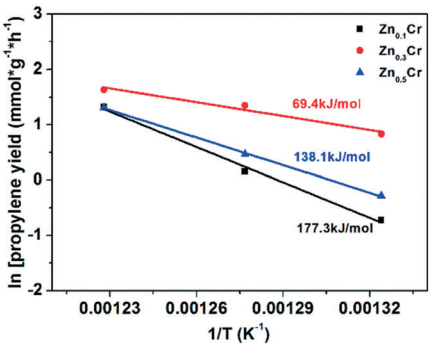


Fig. 7 Arrhenius plots for estimating the apparent activation energy of the PDH reaction over Zn/Cr catalysts with different ratios.

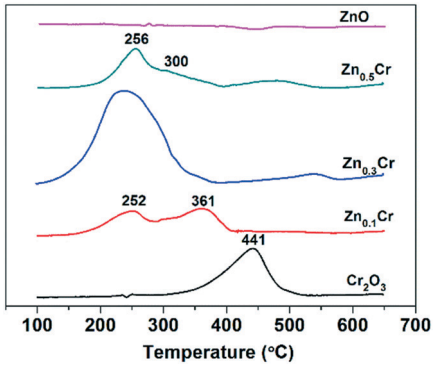


Fig. 8 $H_2$-TPR profiles of $Zn_xCr$ along with those of single component catalysts.

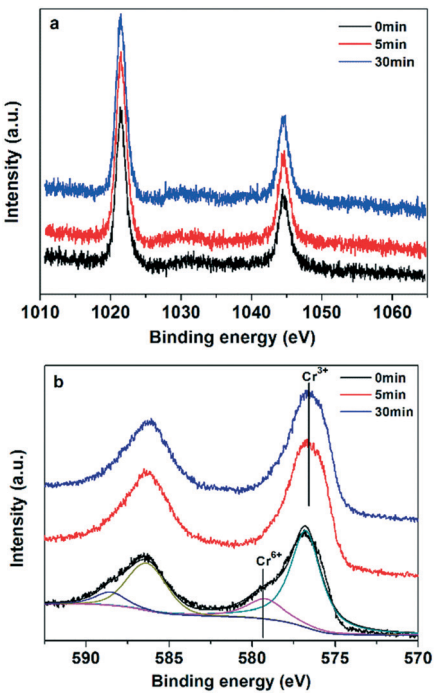


Fig. 9 *In situ* XPS spectra taken before propane was fed in (0 min) and after the reaction had been allowed for 5 and 30 min: (a) Zn 2p; (b) Cr 2p.

reaction for 30 min exhibits a similar feature and there is not much change with respect to that for 5 min. These results indicate that some $Cr^{6+}$ species on the fresh catalyst surface are reduced to $Cr^{3+}$ during the initial stage of the PDH reaction and remain as $Cr^{3+}$ during the reaction. The reduction of $Cr^{6+}$ to $Cr^{3+}$ species during the initial stage of the PDH reaction was also observed by *in situ* XANES and UV-vis spectroscopy previously.[38,39] De Rossi *et al.* reported a correlation of the concentration of the coordinatively unsaturated $Cr^{3+}$ species with the PDH activity over $Cr/Al_2O_3$ and $Cr/SiO_2$ catalysts.[11] They further concluded that the most active $Cr^{3+}$ species were those with two coordinative vacancies, according to the IR studies of CO and NO adsorption on $Cr/SiO_2$.[11] In this work, we observe some reducible $Cr^{6+}$ species on the surface. However, the presence of coordinatively unsaturated $Cr^{3+}$ on the defect sites of $Cr_2O_3$ and small particles of $ZnCr_2O_4$, and even their interfaces cannot be excluded completely. These may have led to a lower apparent activation energy for $Zn_{0.3}Cr$ than the other two catalysts, and hence enhanced its PDH activity.

## Conclusions

We report here that $Cr_2O_3$ promoted with zinc has remarkably enhanced its catalytic activity in the PDH reaction. Furthermore, this enhancement is dependent on the molar ratio of Zn/Cr and $Zn_{0.3}Cr$ exhibits the highest activity and selectivity to propylene. For instance, propane conversion reaches 31.3% and propylene selectivity is 94% under reaction conditions of 480 °C, 0.1 MPa, 5% $C_3H_8$/Ar and a space velocity of 5000 ml $h^{-1}$ $g_{cat}^{-1}$. In comparison, propane conversion is only 7% and propylene selectivity is 92% over $Zn_{0.1}Cr$ and 11% and 93% over $Zn_{0.5}Cr$, respectively. All are higher than those over the single component catalysts $Cr_2O_3$ and ZnO. XRD, TEM, $NH_3$-TPD, XPS and $H_2$-TPR indicate that $Zn_{0.3}Cr$ contains small spinel particles, which could lead to formation of more defect sites around $ZnCr_2O_4$ particles and/or their interfaces with $Cr_2O_3$ though the latter phase still retains a large particle size. Furthermore, the lowest apparent activation energy over $Zn_{0.3}Cr$ implies that the Zn additive may have also modified the properties of the active sites.

## Conflicts of interest

There are no conflicts to declare.

## Notes and references

1 F. Zhang, R. Wu, Y. Yue, W. Yang, S. Gu, C. Miao, W. Hua and Z. Gao, *Microporous Mesoporous Mater.*, 2011, **145**, 194–199.
2 L. Li, W. Zhu, L. Shi, Y. Liu, H. Liu, Y. Ni, S. Liu, H. Zhou and Z. Liu, *Chin. J. Catal.*, 2016, **37**, 359–366.
3 Y. Ren, F. Zhang, W. Hua, Y. Yue and Z. Gao, *Catal. Today*, 2009, **148**, 316–322.
4 L. Deng, T. Shishido, K. Teramura and T. Tanaka, *Catal. Today*, 2014, **232**, 33–39.
5 N. Zeeshan, *Rev. Chem. Eng.*, 2015, **31**, 413–436.
6 P. Tian, Y. Wei, M. Ye and Z. Liu, *ACS Catal.*, 2015, **5**, 1922–1938.
7 T. Otroshchenko, S. Sokolov, M. Stoyanova, V. A. Kondratenko, U. Rodemerck, D. Linke and E. V. Kondratenko, *Angew. Chem., Int. Ed.*, 2015, **54**, 15880–15883.
8 G. Wang, H. Zhang, H. Wang, Q. Zhu, C. Li and H. Shan, *J. Catal.*, 2016, **344**, 606–608.
9 F. E. Frey and W. F. Huppke, *Ind. Eng. Chem. Res.*, 1933, **25**, 54–59.
10 B. M. Weckhuysen and R. A. Schoonheydt, *Catal. Today*, 1999, **51**, 223–232.
11 S. De Rossi, G. Ferraris, S. Fremiotti, E. Garrone, G. Ghiotti, M. C. Campa and V. Indovina, *J. Catal.*, 1994, **148**, 36–46.
12 S. De Rossi, G. Ferraris, S. Fremiotti, A. Cimino and V. Indovina, *Appl. Catal., A*, 1992, **81**, 113–132.

13 K. L. Fujdala and T. D. Tilley, *J. Catal.*, 2003, **218**, 123–134.
14 A. Węgrzyniak, A. Rokicińska, E. Hędrzak, B. Michorczyk, K. Zeńczak-Tomera, P. Kuśtrowski and P. Michorczyk, *Catal. Sci. Technol.*, 2017, **7**, 6059–6068.
15 J. Sattler, J. Ruiz-Martinez, E. Santillan-Jimenez and B. M. Weckhuysen, *Chem. Rev.*, 2014, **114**, 10613–10653.
16 S. Sokolov, M. Stoyanova, U. Rodemerck, D. Linke and E. V. Kondratenko, *Catal. Sci. Technol.*, 2014, **4**, 1323–1332.
17 M. W. Schreiber, C. P. Plaisance, M. Baumgartl, K. Reuter, A. Jentys, R. Bermejo-Deval and J. A. Lercher, *J. Am. Chem. Soc.*, 2018, **140**, 4849–4859.
18 T. P. Otroshchenko, V. A. Kondratenko, U. Rodemerck, D. Linke and E. V. Kondratenko, *Catal. Sci. Technol.*, 2017, **7**, 4499–4510.
19 C. Chen, M. Sun, Z. Hu, J. Ren, S. Zhang and Z. Y. Yuan, *Catal. Sci. Technol.*, 2019, **9**, 1979–1988.
20 C. Chen, Z. Hu, J. Ren, S. Zhang, Z. Wang and Z. Y. Yuan, *ChemCatChem*, 2019, **11**, 868–877.
21 N. M. Schweitzer, B. Hu, U. Das, H. Kim, J. Greeley, L. A. Curtiss, P. C. Stair, J. T. Miller and A. S. Hock, *ACS Catal.*, 2014, **4**, 1091–1098.
22 S. Tian, Y. Wu, K. Li, H. Xie, H. Ren, Y. Zhao, Z. Miao and Y. Tan, *Energy Technol.*, 2018, **6**, 1805–1812.
23 F. Al-Wadaani, E. F. Kozhevnikova and I. V. Kozhevnikov, *Appl. Catal., A*, 2009, **363**, 153–156.
24 M. Bertoldi, B. Fubini and E. Giamello, *J. Chem. Soc., Faraday Trans.*, 1988, **84**, 1405–1421.
25 X. Q. Gao, W. D. Lu, S. Z. Hu, W. C. Li and A. H. Lu, *Chin. J. Catal.*, 2019, **40**, 184–191.
26 C. Fang, D. Zhang, S. Cai, L. Zhang, L. Huang, H. Li, P. Maitarad, L. Shi, R. Gao and J. Zhang, *Nanoscale*, 2013, **5**, 9199–9207.
27 S. Tian, Y. Wu, H. Ren, H. Xie, Y. Zhao, Q. Ma, Z. Miao and Y. Tan, *Fuel Process. Technol.*, 2019, **193**, 53–62.
28 S. Tian, S. Wang, Y. Wu, J. Gao, Y. Bai, P. Wang, H. Xie, Y. Han and Y. Tan, *J. Mol. Catal. A: Chem.*, 2015, **404–405**, 139–147.
29 X. Gao, Y. Wu, G. Yang, T. Zhang, X. Li, H. Xie, J. Pan and Y. Tan, *Appl. Catal., A*, 2017, **547**, 1–11.
30 S. A. Hosseini, M. C. Alvarez-Galvan, J. L. G. Fierro, A. Niaei and D. Salari, *Ceram. Int.*, 2013, **39**, 9253–9261.
31 B. Grzybowska, J. Słoczyński, R. Grabowski, K. Wcisło, A. Kozłowska, J. Stoch and J. Zieliński, *J. Catal.*, 1998, **178**, 687–700.
32 V. Akula, R. Sarkari, A. Chatla, K. Vankudoth and K. K. Mandari, *Appl. Catal., A*, 2012, **441–442**, 108–118.
33 F. Simard, U. A. Sedran, J. Sepúlveda, N. S. Fígoli and H. I. de Lasa, *Appl. Catal., A*, 1995, **125**, 81–98.
34 X. Gao, Y. Wu, T. Zhang, L. Wang, X. Li, H. Xi and Y. Tan, *Catal. Sci. Technol.*, 2018, **8**, 2975–2986.
35 H. Yang, L. Xu, D. Ji, Q. Wang and L. Lin, *Catal. Lett.*, 2002, **76**, 151–159.
36 W. Huang, W. Zha, D. Zhao and S. Feng, *Solid State Sci.*, 2019, **87**, 49–52.
37 V. Z. Fridman, R. Xing and M. Severance, *Appl. Catal., A*, 2016, **523**, 39–53.
38 M. S. Kumar, N. Hammer, M. Ronning, A. Holmen, D. Chen, J. Walmsley and G. Oye, *J. Catal.*, 2009, **261**, 116–128.
39 P. Michorczyk, J. Ogonowski and K. Zeńczak, *J. Mol. Catal. A: Chem.*, 2011, **349**, 1–12.